Global Climate System

Clouds and aerosols in the climate system

Peter Kuma[1,*]

24 January 2023

[1]Stockholm University, Stockholm, Sweden
*peter.kuma@misu.su.se, https://peterkuma.net

Based in part on slides by F. Bender (2021).

Introduction

- Clouds and aerosols have a major effect on Earth's radiation budget.
- They are highly spatially and temporally variable and have highly variable properties. Hence, they are very difficult to simulate and observe accurately.

CERES 25 January 2020, daily mean
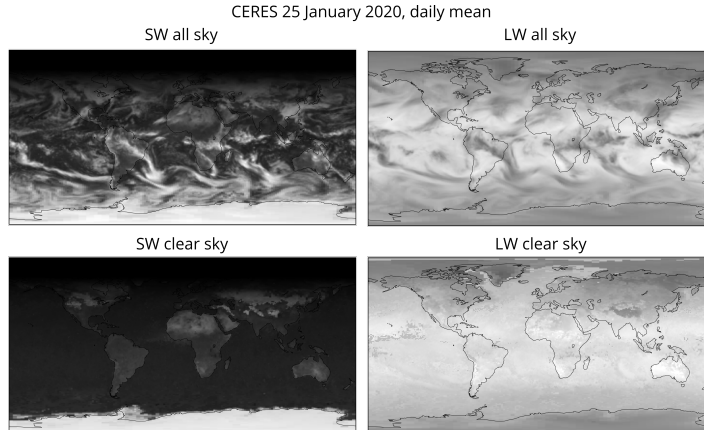
Figure: Daily mean of outgoing top of atmosphere (TOA) shortwave (SW) and longwave (LW) radiation.

Introduction (cont.)

- Currently clouds are the main source of uncertainty in future climate projections.
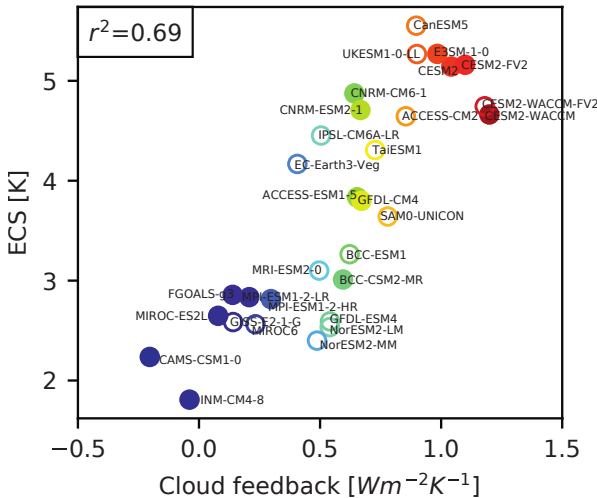
Figure: Scatter plot of equilibrium climate sensitivity (ECS) and cloud feedback. Adopted from Wang et al. (2021).

Earth's energy budget
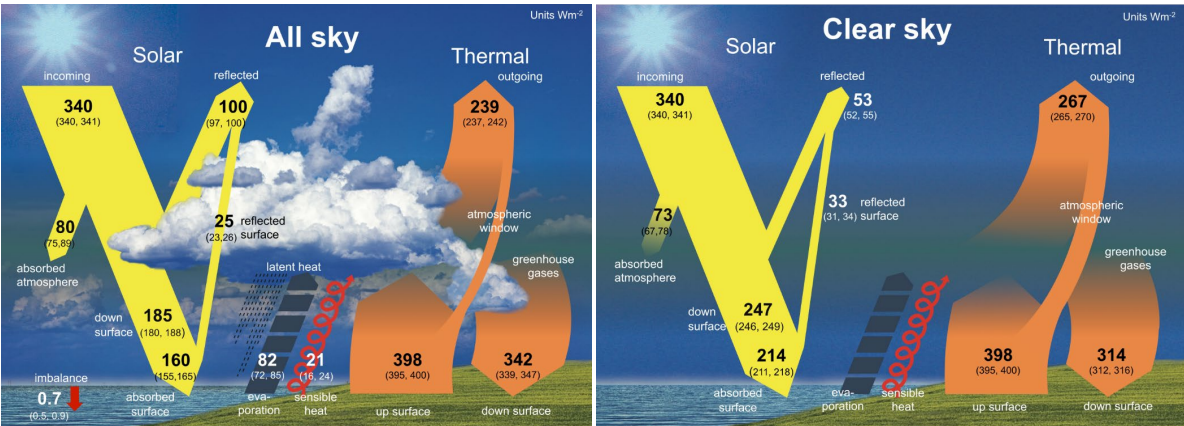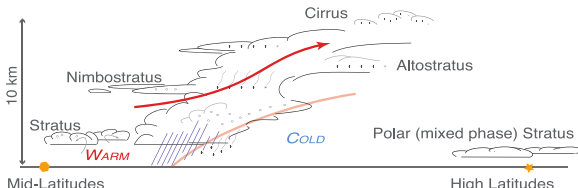
Figure: (left) Schematic representation of the global mean energy budget of the Earth, and **(right)** its equivalent without considerations of cloud effects. Adopted from IPCC AR6.

Cloud properties

- Clouds have a large number of physical properties affecting the climate: Cloud genus, cloud fraction, altitude, phase (liquid, ice or mixed), liquid water content, ice content, cloud droplet and ice crystal size distribution, ice crystal habit, lifetime, geometrical thickness, number of layers, ...
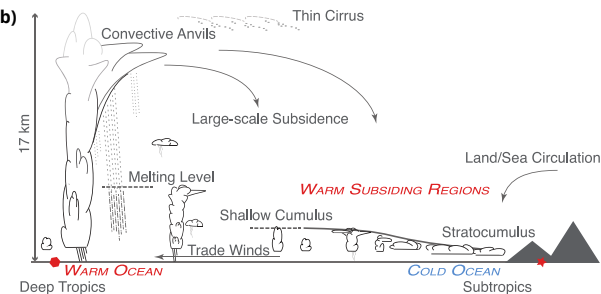
Figure: Diverse cloud regimes reflect diverse meteorology. A schematic **(a)** through a typical warm front of an extratropical cyclone, **(b)** along the low-level trade wind flow from a subtropical west coast of a continent to the ITCZ. Adopted from IPCC AR5.

Global distribution of clouds

- Clouds cover about 2/3 of the globe. They are particularly dense over the poles and the ITCZ.
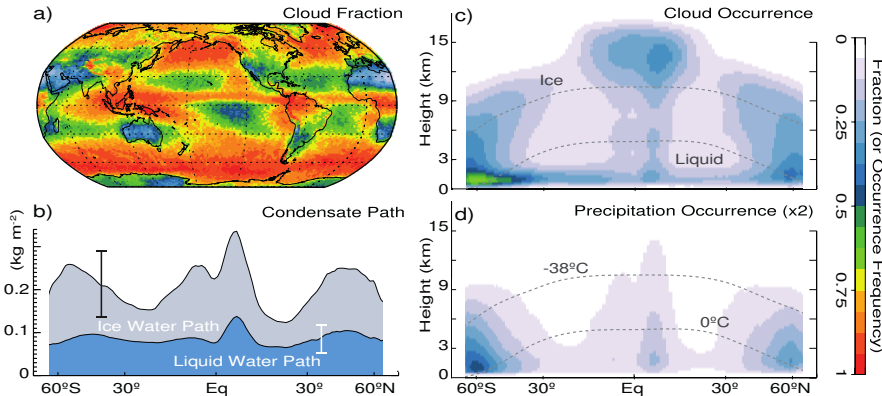

Figure: (a) Annual mean cloud fractional occurrence (CloudSat/CALIPSO 2B-GEOPROF-LIDAR data set for 2006–2011; Mace et al., 2009). **(b)** Annual zonal mean liquid water path (blue shading, microwave radiometer data set for 1988–2005 from O'Dell et al. (2008)) and total water path (ice path shown with gray shading, from CloudSat 2C-ICE data set for 2006–2011 from Deng et al. (2010) over oceans). **(c–d)** latitude–height sections of annual zonal mean cloud (including precipitation falling from cloud) occurrence and precipitation (attenuation-corrected radar reflectivity >0 dBZ) occurrence; the latter has been doubled to make use of a common colour scale (2B-GEOPROF-LIDAR data set). The dashed curves show the annual mean 0°C and −38°C isotherms. Adopted from IPCC AR5.

Clouds and radiation

- Clouds interact with radiation by scattering and absorbing solar (shortwave) and terrestrial (longwave) radiation, and emitting longwave radiation.
- This is represented as part of volume scattering coefficient (β_s) and volume absorption coefficient (β_a) in the radiative transfer equation (RTE):

$$\mathrm{d}I(\Omega) = -\beta_e \mathrm{d}s I(\Omega) + \beta_a \mathrm{d}s B(\Omega) + \beta_s \mathrm{d}s \frac{1}{4\pi} \int_{4\pi} p(\Omega', \Omega) I(\Omega') \mathrm{d}\omega'$$
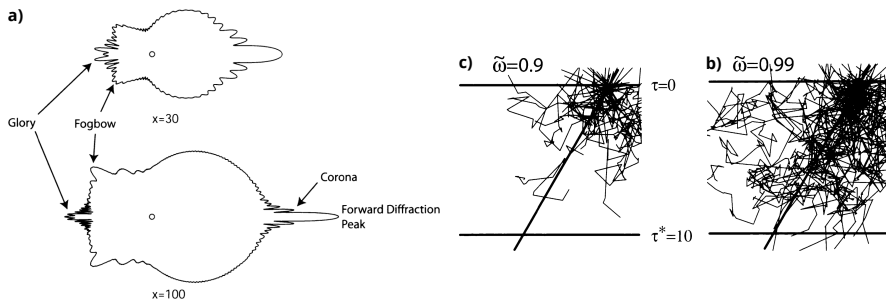
Figure: (a) Polar plots of the Mie-derived scattering phase function p(Ω) for selected values of x, plotted as $\log[p(\Omega)]$. **(b, c)** Examples of the random paths of 100 photons in a plane-parallel, isotropically scattering layer (g = 0) with optical thickness $\tau^* = 10$ and variable single scatter albedo $\tilde{\omega}$. Adapted from Petty (2006).

Cloud radiative effect (CRE)

- Shortwave and longwave cloud radiative effect (CRE), also called cloud radiative forcing (CRF), is defined as:

$$\text{CRE}_{SW} = F^{\uparrow}_{TOA,SW,CS} - F^{\uparrow}_{TOA,SW}$$

$$\text{CRE}_{LW} = F^{\uparrow}_{TOA,LW,CS} - F^{\uparrow}_{TOA,LW}$$

where $F^{\uparrow}_{TOA}$ means upward radiation flux at top of atmosphere (TOA), SW and LW denote shortwave and longwave component (respectively), and CS denotes clear sky flux. Negative CRE means cooling of the climate, positive CRE means warming of the climate. Clear sky flux is calculated by artificially removing clouds from a grid cell in a radiative transfer model, without otherwise affecting running of the model.
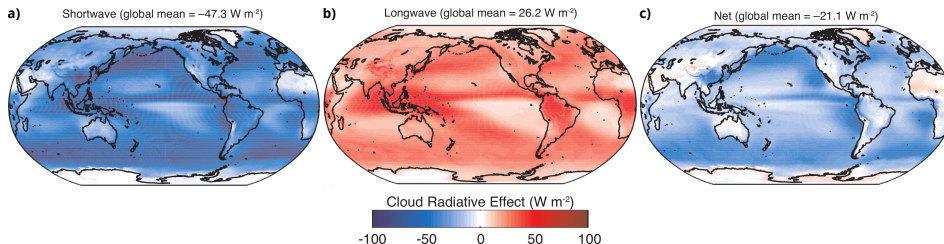

Figure: Distribution of annual-mean top of the atmosphere (a) shortwave, (b) longwave, (c) net cloud radiative effects averaged over the period 2001–2011 from the Clouds and the Earth's Radiant Energy System (CERES) Energy Balanced and Filled (EBAF) Ed2.6r data set (Loeb et al., 2009). Adopted from IPCC AR5.

Cloud radiative kernels

- Cloud radiative kernels quantify how change of cloud occurrence affects cloud radiative forcing, binned by cloud top pressure and cloud optical depth.

- Clouds have warming effect in LW and cooling effect in SW. The net effect is that they have overall cooling effect for low-, mid-level clouds and thick high clouds, and warming effect for thin high clouds.
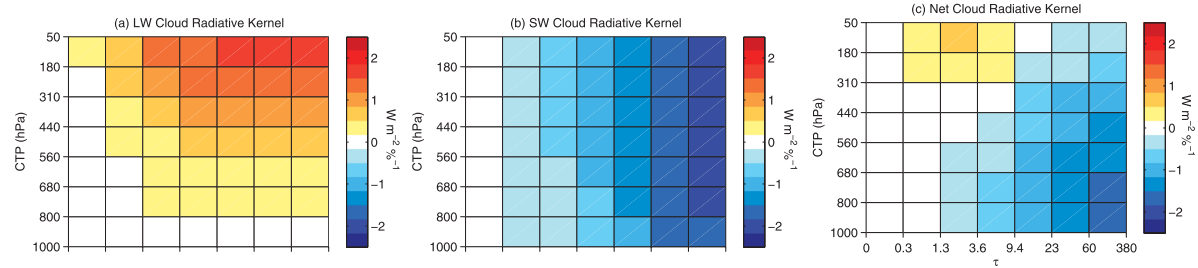

Figure: Global, annual, and ensemble mean (a) LW, (b) SW, and (c) net cloud radiative kernels. Adopted from Zelinka et al. (2012).

Cloud phase

- Cloud have different effect on radiation depending on their phase.
- Warm clouds can occur at T > -38°C, are composed liquid droplets and scatter radiation in the Mie regime, cold clouds can occur at T < 0°C, are composed of ice crystals of various *habits*, scatter and absorb radiation in a complex way, mixed clouds can occur at -38°C < T < 0°C, are composed of liquid and ice and are very hard to simulate correctly in models.
- Supercooled liquid water (SLW) clouds are warm and mixed clouds at T < 0°C. They are very common in the Southern Ocean.
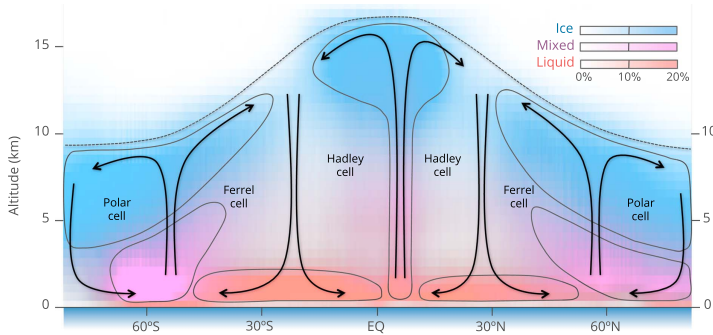

Figure: Conceptual illustration of the location of mixed-phase clouds. Adapted from Matus and L'Ecuyer (2017).

Cloud phase (cont.)

- Ice crystals are larger than cloud droplets and have a smaller area–to–volume ratio. Because scattering is proportional to the cross-sectional area, they scatter less radiation for the same amount of water (the refractive index, density and scattering regime are also different).

- Ice crystals can have various habits depending on temperature and supersaturation. Moreover, ice plates can become horizontally aligned, changing how radiation is scattered.
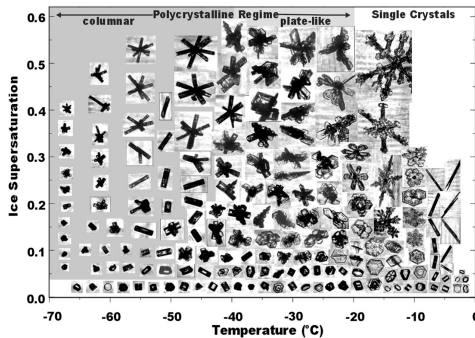

Figure: Habit diagram for atmospheric ice crystals derived from laboratory results (BH04) and CPI images gathered during AIRS II and other field studies. Adapted from Bailey and Hallett (2009).

Cloud droplet size distribution

- Cloud droplet size distribution is usually approximated by a Gamma or log-normal size distribution.

- Characterised by *effective radius*, which defines the integrated effect on radiation. It is defined as the third over the second moment of the size distribution (r is the radius and n is the PDF):

$$r_{\text{eff}} = \frac{\int_0^\infty r^3 n(r)\mathrm{d}r}{\int_0^\infty r^2 n(r)\mathrm{d}r}$$

- Effect on radiation depends on the cross-sectional area (second moment), the third moment corresponds to the volume and mass.
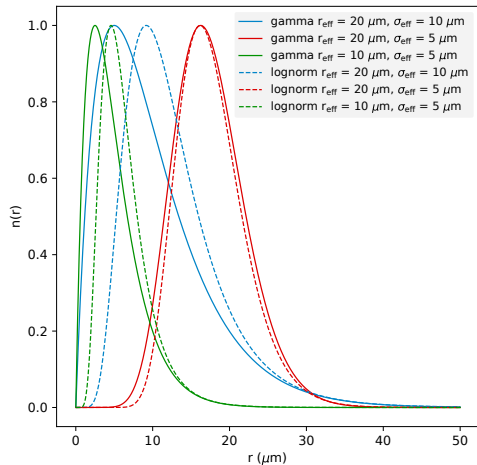

Figure: Theoretical distributions of cloud droplet radius based on the log-normal and Gamma distributions parametrised by multiple choices of the effective radius r_{eff} and effective standard deviation σ_{eff}. Adapted from Kuma et al. (2021).

Clouds in climate models

- Clouds in current climate models are mostly represented by subgrid-scale processes.

- Model clouds might be distinguished into *large-scale* and subgrid-scale, or *stratiform* and *convective*.

- Can be *prognostic* (cloud state is persists across time step) or *diagnostic* (cloud state is derived from other fields in each time step).

- Per grid cell and level variables: cloud fraction ('cl', %), cloud liquid mixing ratio ('clw', gg^{-1}), ice mixing ratio ('cli', gg^{-1}). [CMIP model output variable names and units are in parentheses.]
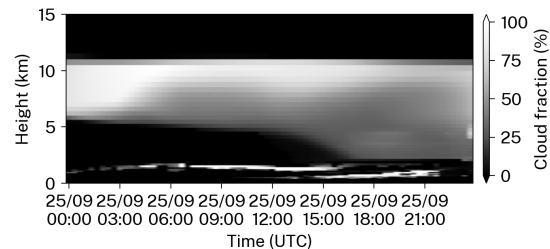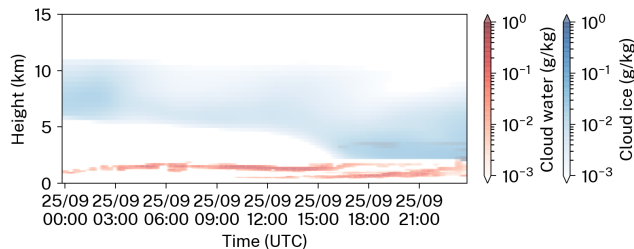

Figure: Example of model cloud representation in the Unified Model (UM). Adapted from Kuma et al. (2021).

Clouds in climate models (cont.)

(This applies to the Unified Model (UM), other models may differ.)

- Cloud fraction corresponds to a fraction of a grid cell which has relative humidity (RH) over critical RH, which depends on the amount of supersaturation required for condensation. Specific humidity within a grid cell is represented by a probability distribution.

- Clouds form by large-scale (grid resolved) ascending air, diabatic cooling, and subgrid-scale convective plumes (*mass flux* and turbulence parametrisation).

- Clouds are destroyed by descending air, diabatic warming, *autoconversion* (conversion to precipitation), and turbulent mixing.
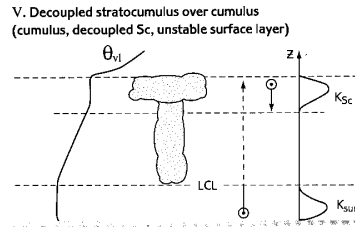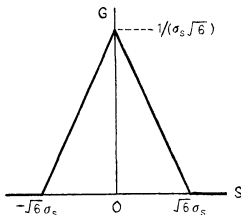

Figure: (left) The symmetric triangular probability distribution function with standard deviation σ_s, used in the cloud model. Adapted from Smith (1990). **(right)** Schematic representation of a boundary layer type. Adapted from Lock et al. (2000).

Cloud feedback

- Cloud feedback α_C is the change of global mean cloud radiative effect with global mean near-surface air temperature. It has units $Wm^{-2}K^{-1}$. Positive if clouds amplify warming, negative if they dampen warming.

- Due to changes in cloud amount, albedo (e.g. due to cloud phase change), height, ...
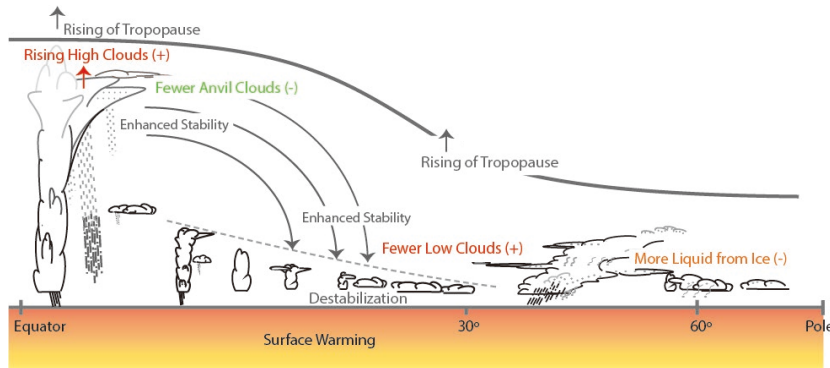
Figure: Schematic cross section of diverse cloud responses to surface warming from the tropics to polar regions. Adapted from IPCC AR6.

Cloud feedback (cont.)

- Cloud feedback is the most uncertain climate feedback. Best estimate 0.42 $Wm^{-2}K^{-1}$, likely range 0.12–0.72 $Wm^{-2}K^{-1}$ (IPCC AR6).

- Positive contribution is from cloud height change increase and reduction of cloud amount, negative contribution is from tropical anvil area.
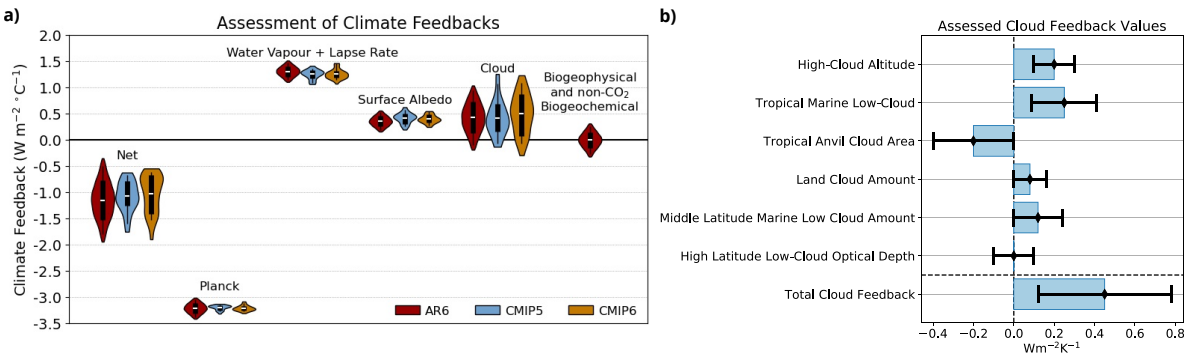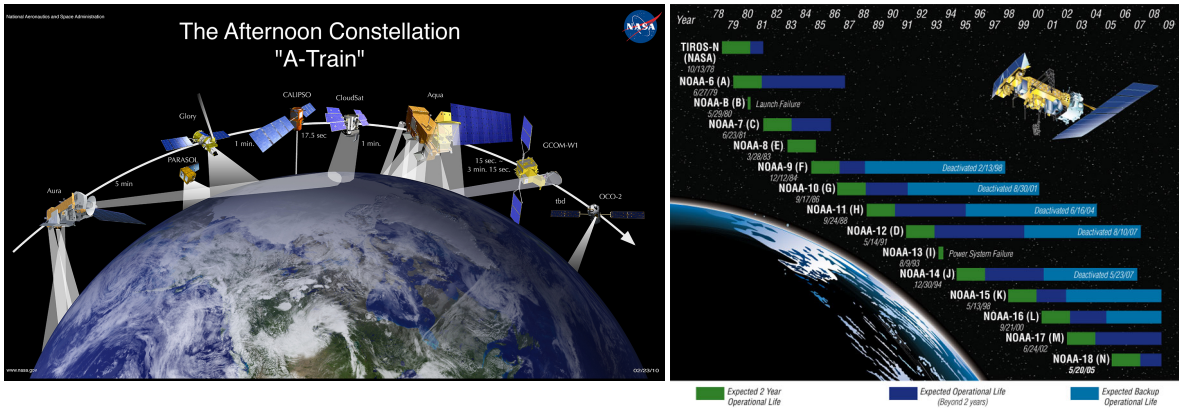

Figure: (a) Global-mean climate feedbacks estimated in abrupt4xCO2 simulations of 29 CMIP5 models (light blue) and 49 CMIP6 models (orange), compared with those assessed in this Report (red). Adopted from IPCC AR6. **(b)** Assessed values of individual cloud feedbacks and the total cloud feedback based upon process evidence. Adopted from Sherwood et al. (2020).

Satellite observations of clouds

- Satellite platforms: *geosynchronous* (*geostationary*), *polar-orbiting*, L2 Lagrange point (DSCOVR EPIC).

- Satellite *series* (satellite iterations carrying similar instruments): TIROS/NOAA/ESA polar satellites (AVHRR imager), NASA Nimbus.

- Satellite *constellations* (satellites carrying different instruments flying in a formation): NASA/CNES/JAXA A-train.

Satellite observations of clouds (cont.)

- *Passive imaging* instruments measure commonly radiation with a scanning spectrometer. Pros: wide swath, many bands (wavelengths), long historical record. Cons: 2D view of clouds, little information about cloud profile. Example: Moderate Resolution Imaging Spectroradiometer (MODIS) on Terra and Aqua, Clouds and the Earth's Radiant Energy System (CERES).

- *Passive sounding* instruments can measure vertically integrated quantities, such as total cloud water content, by using the microwave spectrum. Example: Special Sensor Microwave Imager (SSM/I).

- *Active* instruments are radars and lidars: Cloud Profiling Radar (CPR) on CloudSat, Cloud-Aerosol Lidar and Infrared Pathfinder Satellite Observation (CALIPSO), Cloud-Aerosol Transport System (CATS) on the ISS, EarthCARE. Pros: cloud profile information. Cons: narrow swath, short historical record (2006–present).
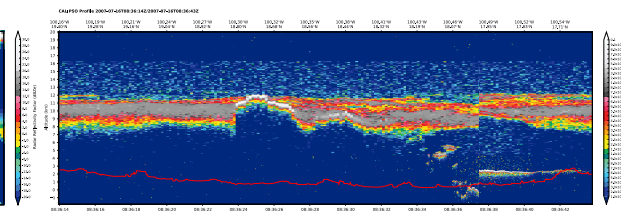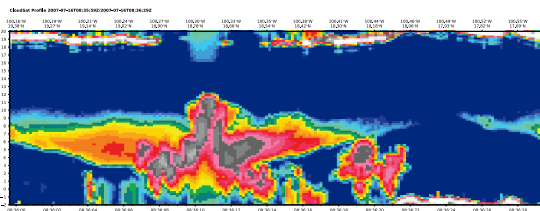

Figure: Profile of a cloud as observed by **(a)** CloudSat (radar) and **(b)** CALIPSO (lidar). Adopted from Kuma (2010).

Satellite cloud datasets

- Geosynchronous satellites: International Satellite Cloud Climatology Project (ISCCP).
- Polar satellites (NOAA/ESA): Cloud_cci, 'The CM SAF Cloud, Albedo And Surface Radiation dataset from AVHRR data' (CLARA-A2), 'Pathfinder Atmospheres – Extended' (PATMOS-x).
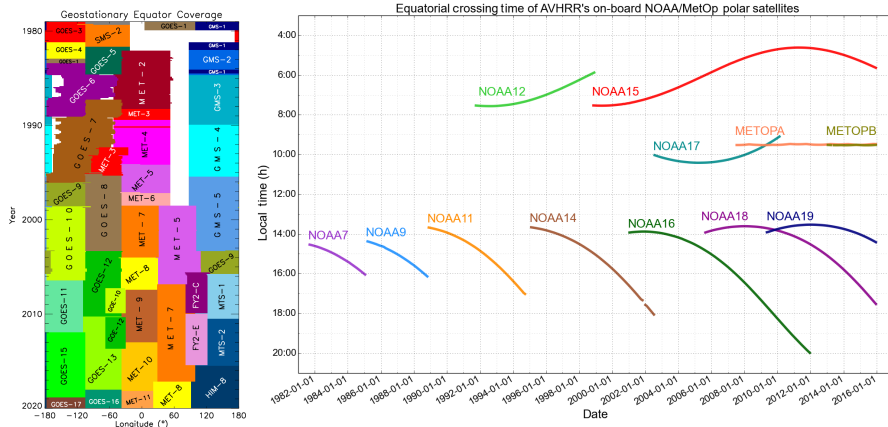

Figure: (left) ISCCP: 'The Geostationary Quilt'. **(right)** Satellites used in CLARA-A2.

Ground-based and in situ observations of clouds

- Clouds can be observed from the ground (or an aircraft) by remote sensing with a lidar, ceilometer, cloud (high frequency) radar, sky camera, microwave radiometer, …. Pros: easy to deploy, long time series, autonomous. Cons: various cloud properties are difficult to infer, limited view.

- In situ observations can be done with an aircraft, meteorological balloon, UAV, rocket, on the ground (if the cloud/fog touches the surface), …. Pros: accurate determination of cloud properties (LWC, IC, size distribution, ice habit, …). Cons: difficult to deploy, short time series/localised observation.

- Networks of stations: E-PROFILE (lidars), Cloudnet (lidar and radar), MPLNET (lidar), ARM (multi-instrument stations), ….
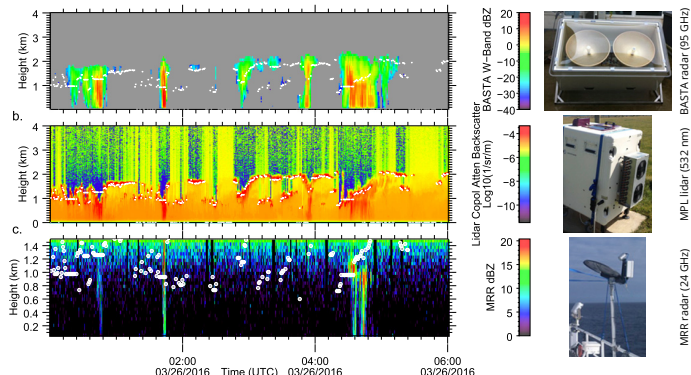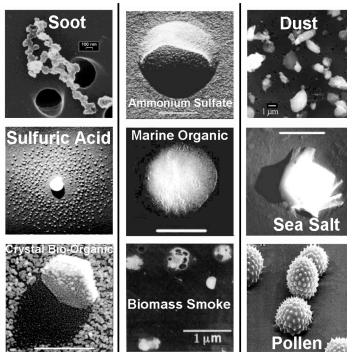

Figure: Active remote sensing measurements collected from R/V Investigator for 0000–0600 UTC 26 Mar 2016, showing **(a)** W-band radar reflectivity factor, **(b)** copolar lidar backscatter, and **(c)** radar reflectivity collected by the K-band MRR. Adapted from Mace and Protat (2018).

Aerosols

- Aerosols are suspended solid and liquid particles in the atmosphere: soot (black carbon), brown carbon (BrC), sulphate, dust, sea salt, biogenic, ammonium, pollen, microplastics, ….

- Natural sources: soil, deserts, forests, oceans, plankton, volcanoes, ….

- Anthropogenic sources: fossil fuel and biofuel burning, biomass burning, industries, plastics and synthetic textiles, tire and brake wear particles, dust from road vehicles.

Images by C. Leck.

Aerosols (cont.)

- Aerosols can be *primary* – emitted directly, or *secondary* – created by reactions in the atmosphere (e.g. gas–to–particle conversion).
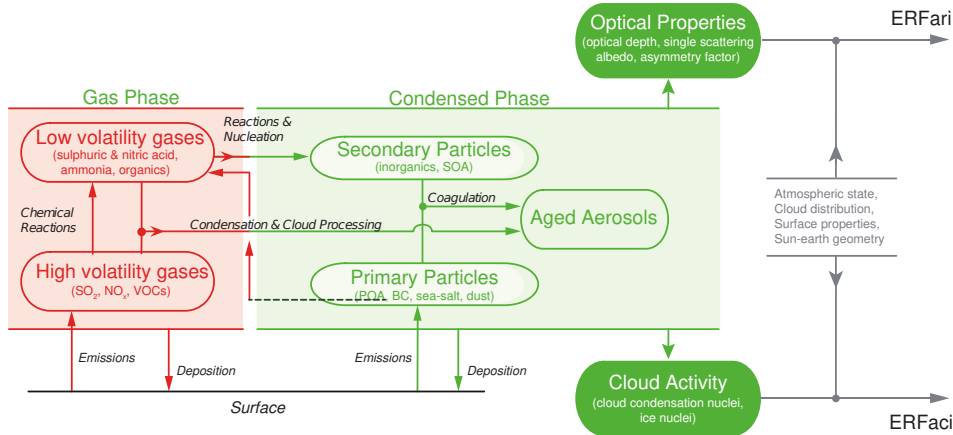

Figure: Overview of atmospheric aerosol and environmental variables and processes influencing aerosol–radiation and aerosol–cloud interactions. Adopted from IPCC AR5.

Global distribution of aerosols

- Aerosols are mostly located in the Northern Hemisphere due to high anthropogenic emissions, but also mineral dust form land – East Asia has the highest aerosol optical depth (AOD) due to industrial activity.
- The Southern Hemisphere has highest AOD over Africa due to biomass burning, and over the Southern Ocean (sea salt and biogenic aerosol).
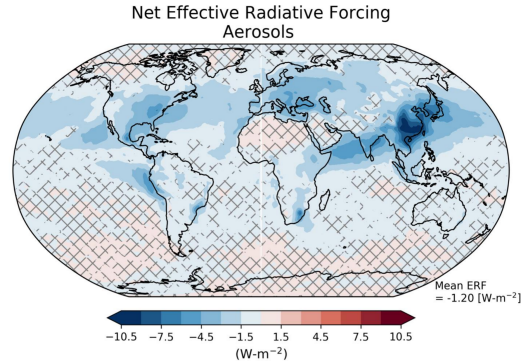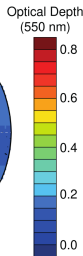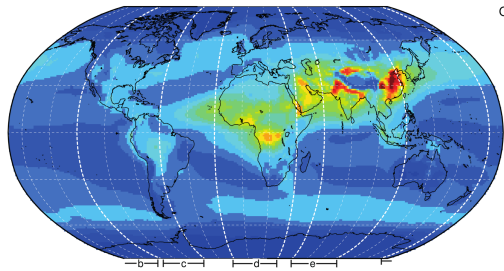

Figure: (left) Spatial distribution of the 550 nm aerosol optical depth (AOD, unitless) from the European Centre for Medium Range Weather Forecasts (ECMWF) Integrated Forecast System model with assimilation of Moderate Resolution Imaging Spectrometer (MODIS) aerosol optical depth (Benedetti et al., 2009; Morcrette et al., 2009) averaged over the period 2003–2010. Adopted from IPCC AR5. **(right)** Multi-model mean effective radiative forcing (ERFs) due to aerosol changes between 1850 and recent-past (1995–2014). Adopted from IPCC AR6.

Aerosol properties

- Aerosol properties include chemical composition, size, water affinity (hygroscopic/hygrophobic), optical properties (refractive index, colour, emissivity), shape, age, vertical distribution, ...
- There is a large number of aerosol types in the atmosphere, large number of sources, complex chemical transformations, condensation, coagulation, scavenging and deposition processes.
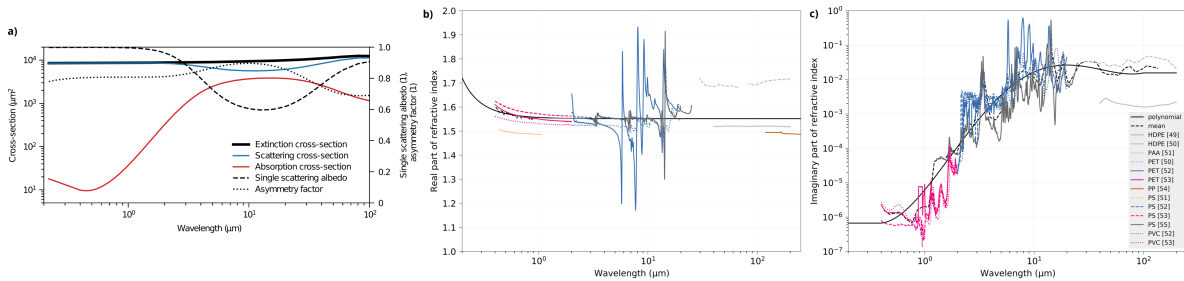

Figure: (a) Optical properties of microplastic fragments, **(b, c)** Refractive index of polymers. Adapted from Revell et al. (2021).

Historical aerosol concentration

- Aerosol concentration has increased rapidly between 1950 and 1980, and then stayed relatively constant.
- 2005–2014 mean aerosol effective radiative forcing −1.1 Wm^{-2} relative to 1750 (Smith et al., 2021)
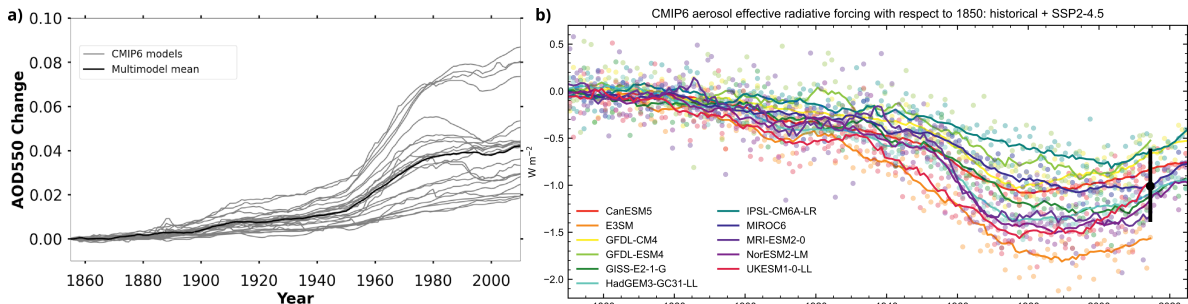

Figure: (a) Time evolution of changes in global mean aerosol optical depth (AOD) at 550 nm. Adopted from IPCC AR6. **(b)** CMIP6 diagnosed net aerosol effective radiative forcing relative to an 1850 climatology. Adopted from Smith et al. (2021).

Historical aerosol concentration (cont.)

- Aerosol partially counteracted warming by greenhouse gases.
- Aerosol concentration is projected to decrease in the future, enhancing global warming.
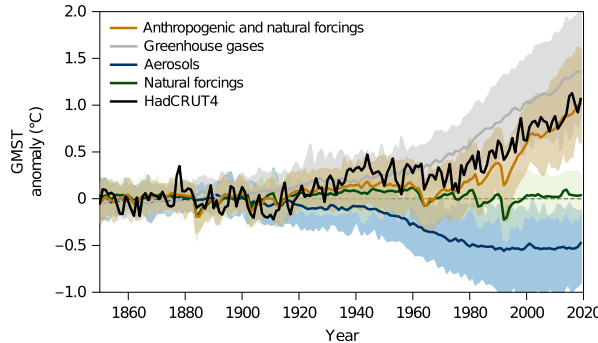

Figure: Comparison of 1850–2019 global mean temperature evolution in observations and CMIP6 simulations. HadCRUT4 GMST compared with: global mean surface temperature (GMST) from CMIP6 historical-ssp245 simulations with anthropogenic and natural forcings, natural forcing simulations, well-mixed greenhouse gas-only simulations and aerosol-only simulations. Adopted from Gillett et al. (2021).

Aerosol size modes

- Atmospheric aerosols span a size range from nm to 100s of µm.

- They generally exhibit a multi-modal size distribution: *nucleation* (ultrafine) (< 10 nm), *Aitken* (10–100 nm), *accumulation* (100 nm–1 µm), *coarse* (1–10 µm) and *supercoarse* (> 10 µm) mode. [The size ranges are approximate.]
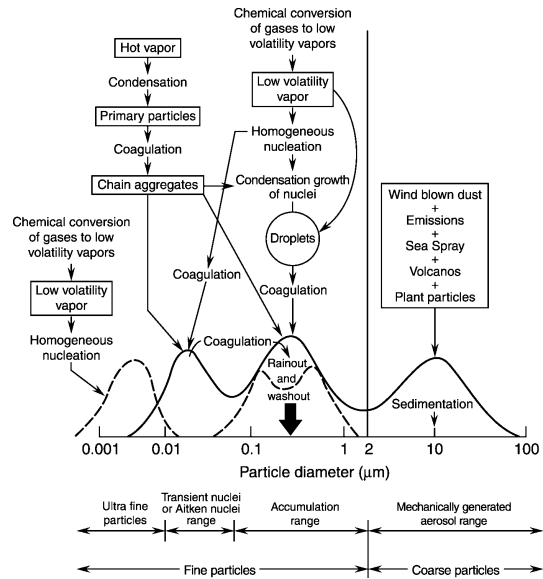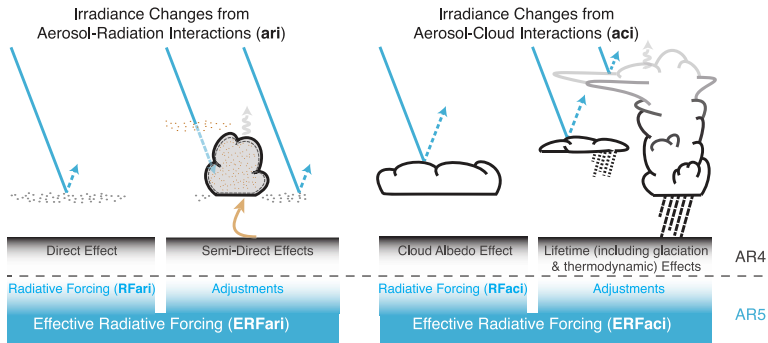
Figure: Schematic of an atmospheric aerosol size distribution. Adopted from Finlayson-Pitts and Pitts (2000).

Aerosols and radiation

- Aerosol impact radiation by a *direct* and *indirect effect* in the atmosphere and by changing albedo of surface ice.
- Direct effect/aerosol–radiation interaction (ari) is through scattering, absorption of shortwave and longwave radiation, and emission of longwave radiation. This may also include adjustment of the climate to the direct affect (*semi-direct effect*).
- Indirect effect/aerosol–cloud interaction (aci) is through acting as cloud condensation nuclei and ice nuclei ('Twomey effect'), changing cloud lifetime and affecting precipitation.

Aerosols radiation interaction (ari) – direct effect

- Aerosols can broadly be separated into 'white' and 'black'. White predominantly scatter radiation, cooling the climate by reflecting solar radiation back to space. Black predominantly absorb radiation, warming the climate. Black aerosol is mostly black carbon (BC) – soot from fossil fuel and biomass burning. White aerosol is most other aerosol, predominantly sulphate aerosol.
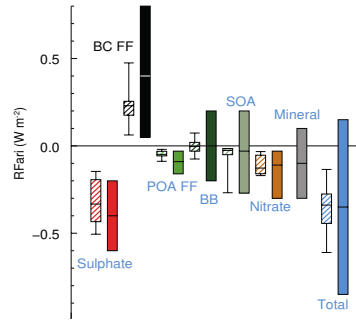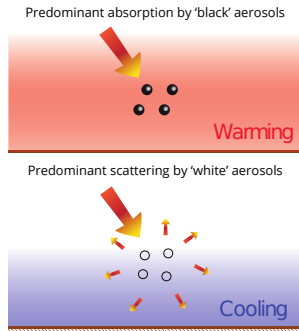
Figure (right): Annual mean top of the atmosphere radiative forcing due to aerosol–radiation interactions (RFari, in Wm^{-2}) due to different anthropogenic aerosol types, for the 1750–2010 period. Abbreviations: black carbon from fossil fuel and biofuel (BC FF), primary organic aerosol (POA), biomass burning (BB), secondary organic aerosol (SOA). Adopted from IPCC AR5.

Aerosols effective radiative forcing (ERF)

- Climate is cooled by sulphate and organic carbon, and warmed by black carbon, but there are large uncertainties.

Effective radiative forcing, 1750 to 2019
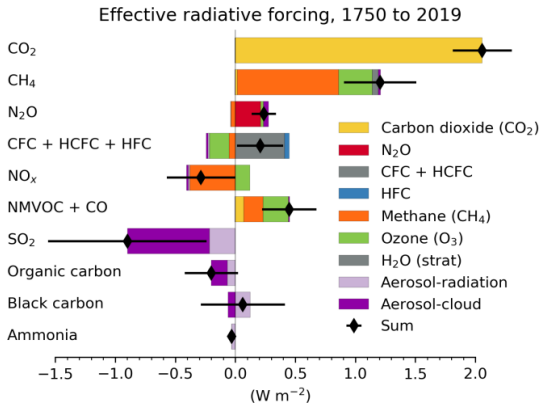
Figure: Contribution to effective radiative forcing (ERF) (left) and global mean surface air temperature (GSAT) change (right) from component emissions between 1750 to 2019 based on CMIP6 models (Thornhill et al., 2021). Adopted from IPCC AR6.

Aerosol–cloud interaction (aci) – indirect effect

- Some aerosols can *activate* – act as *cloud condensation nuclei* (CCN) at a certain supersaturation and aerosol radius. Some aerosol act as *ice nuclei* (IN) on which ice crystals grow. This requires lower supersaturation than homogeneous condensation/deposition, and is the main process behind aerosol–cloud interaction (aci).

- CCN aerosols: sulphate, nitrate, black carbon (when coated), organic aerosol, sea spray. IN aerosols: mineral dust, black carbon, organic aerosol, bacteria, fungal spores and pollen. *Hygroscopic* aerosols are more effective CCN than *hygrophobic*.

- Supersaturation in soluble CCN is determined by Köhler theory: competing effect of concentration (Raoult's law) and droplet curvature (Kelvin effect). Beyond *critical supersaturation*, droplets can continue to grow.
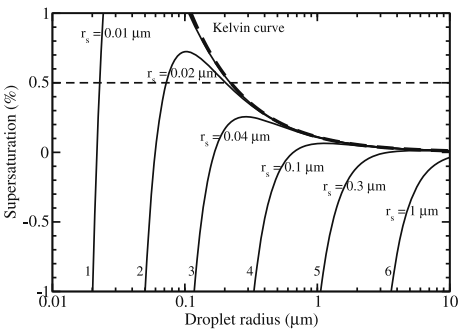
Figure: Supersaturation S (in %) at equilibrium over the surface of a pure water droplet (dashed line) and the surface of water solution droplets containing increasing amounts of soluble matter (solid lines) as a function of the hydrated water droplet radius. The curves are for different values of the radius of the dry aerosol, r_d, which is taken to be ammonium sulphate. Adopted from Boucher (2015).

Aerosols in climate models

- Climate models generally represent mass, number, and size distribution of various aerosol types.
- They interact with radiation (direct effect) and cloud formation (indirect effect).
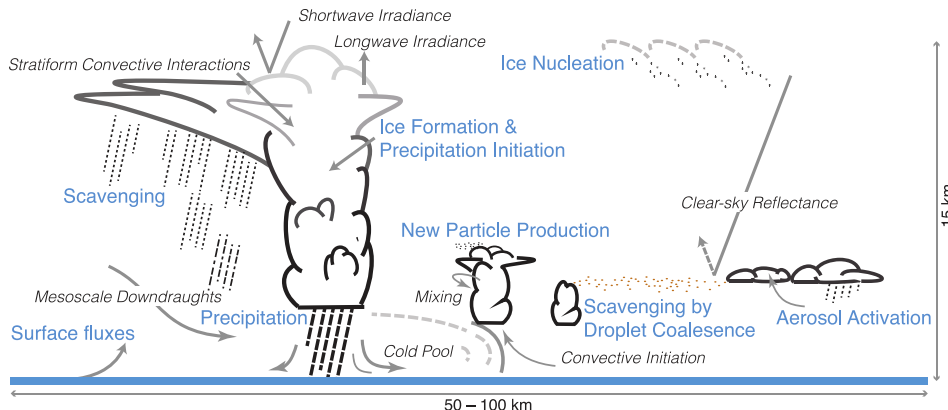
Figure: Schematic depicting the myriad aerosol–cloud–precipitation related processes occurring within a typical GCM grid box. Adopted from IPCC AR5.

Volcanic eruptions

- Major volcanic eruptions produce vast amounts of aerosols, especially SO_2.
- They have a significant cooling effect of the Earth's radiation budget for several years after the eruption.
- They complicate near-term climate prediction (major eruptions are not possible to predict) and comparison of historical record of warming with models.
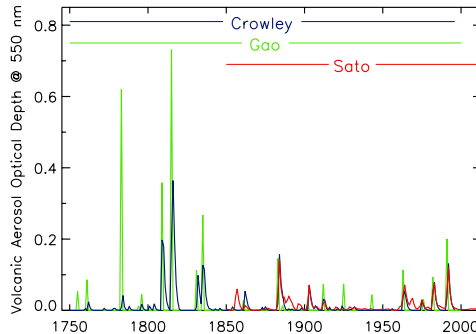
Figure: Volcanic reconstructions of global mean aerosol optical depth (at 550 nm).

Aerosols and human health

- Air pollution is one of the biggest environmental threats to human health, alongside climate change.
- Aerosols contribute to cardiovascular (heart disease and stroke), respiratory disease, lung cancer and other illnesses.
- WHO: In 2019, 99% of the world population was living in places where the WHO air quality guidelines levels were not met. Outdoor air pollution estimated to cause 4.2 mil. premature deaths globally in 2016 (in comparison, COVID-19 caused about 3.5 mil. officially reported deaths in 2021), and 7 mil. if also combined with household air pollution.
- Mostly due to particulate matter (PM) (but other non-aerosol pollutants like ozone contribute).

Pollutant	Averaging Time	2005 AQGs	2021 AQGs
$PM_{2.5}$, $\mu g/m^3$	Annual	10	5
	24-hour[a]	25	15
PM_{10}, $\mu g/m^3$	Annual	20	15
	24-hour[a]	50	45
O_3, $\mu g/m^3$	Peak season[b]	-	60
	8-hour[a]	100	100
NO_2, $\mu g/m^3$	Annual	40	10
	24-hour[a]	-	25
SO_2, $\mu g/m^3$	24-hour[a]	20	40
CO, mg/m^3	24-hour[a]	-	4

Table: Recommended 2021 air quality guidelines (AQG) levels compared to 2005 air quality guidelines. Adopted from WHO AQG 2021.

Aerosols and human health (cont.)

- Particulate matter smaller than 2.5 µm (PM2.5) has the greatest effect on human health. PMs consist of sulphate, nitrates, ammonia, sodium chloride, black carbon, mineral dust and water. PM2.5 can pass through lungs to the blood system. Large particles PM10 (<10 µm) are less damaging.
- WHO (2021): No threshold (for PM) has been identified below which no damage to health is observed.
- Sources of PM: anthropogenic (fossil fuel and biomass burning), natural (dust).
- Between 1960 and 2009 concentrations of PM2.5 globally increased by 38%, due in large part to increases in China and India, with deaths attributable to air pollution increasing by 124% (Shaddick et al., 2020).

0   4   8   12   16   20   24   28   32   36   40   44   48   52   56   60   64   68   72   76   80   84   88   92   96   100+
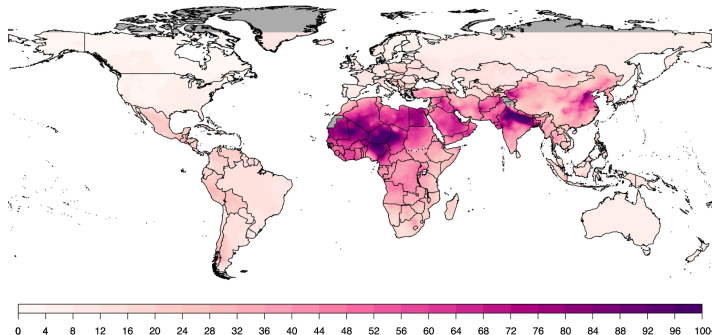
Figure: Map of global PM2.5 (µg/m3) in 2016. Adopted from Shaddick et al. (2020).

Satellite observations of aerosols

- *Passive* imagers – MODIS (Aqua and Terra), AVHRR and VIIRS (NOAA/ESA series), MISR (Terra), SLSTR (Sentinel-3), geosynchronous satellites.
- *Active* instruments – lidar (CALIPSO, CATS, EarthCARE).
- Occultation measurement of aerosol optical depth (AOD).
- Inferred properties (may be limited to clear sky and particular surface type, ocean or land): AOD, aerosol size distribution, aerosol type.

Suomi NPP VIIRS High Quality Aerosol Optical Thickness at 550 nm JPSS EPS
17 Jan 2022

AOT at 550 nm
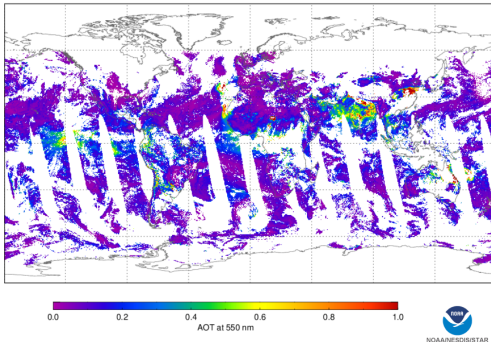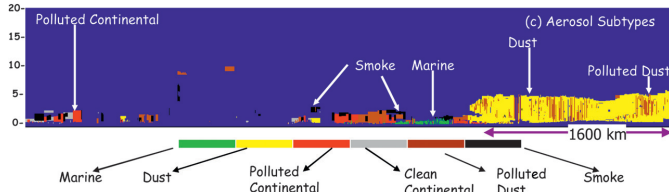
Figure: (left) Daily mean satellite-derived AOD. **(bottom)** Aerosol types inferred from CALIPSO lidar backscatter. Adopted from Omar et al. (2009).

Ground-based and in situ observations of aerosols

- Platforms: land stations, ship, aircraft, balloon, UAV, ...
- Remote sensing: lidar, ceilometer, sun photometer (AOD measurement), ...
- In situ: direct air sampling and subsequent laboratory analysis, filtration, with a *optical particle counter* (OPC), *condensation particle counter* (CPC), ...
- Networks of stations: AERONET, EARLINET, ARM (multi-instrument stations), operational air quality stations (particulate matter), ...

a) MICROTOPS II Sun photometer

b) Alphasense optical particle counter (OPC)

c) 2019-06-10 target classification using lidar, cloud radar, and microwave radiometer
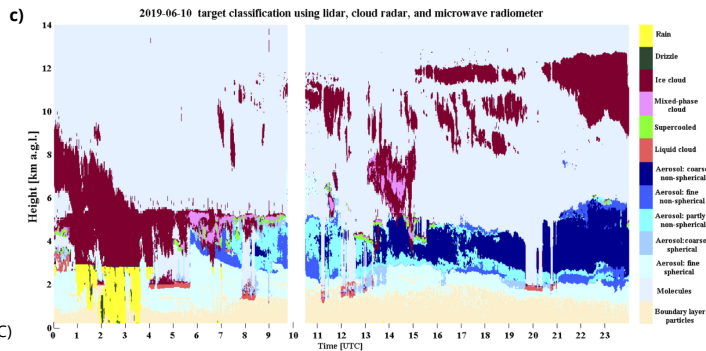
Figure: Examples of instruments and remote sensing **(a)** Sun photometer for measurement of AOD (photo solarlight.com), **(b)** optical particle counter for measurement of particulate matter (photo alphasense.com), **(c)** Synergy for molecule, aerosol and cloud identification derived from a combination of EMORAL Raman-polarization lidar, BASTA Doppler cloud radar, and HATPRO-G2 microwave radiometer over the PolWET site in Rzecin on 10 June 2019. Adopted from Wang et al. (2020).

Further reading

- IPCC AR5 WGI (2013). Chapter 7: Clouds and Aerosols; Chapter 8: Anthropogenic and Natural Radiative Forcing.
- IPCC AR6 WGI (2021). Chapter 6: Short-lived climate forcers; Chapter 7: The Earth's energy budget, climate feedbacks, and climate sensitivity.
- Wallace and Hobbs (2006). Atmospheric Science: An Introductory Survey (2nd Ed.). Chapter 5: Atmospheric Chemistry.
- Boucher (2015). Atmospheric Aerosols Properties and Climate Impacts.
- ESA Earth Observation Portal (eoPortal), `https://eoportal.org`.
- Petty (2006). A first course in atmospheric radiation (2nd Ed.).
- Ahrens and Henson (2021). Meteorology Today: An Introduction to Weather, Climate, and the Environment.
- Kramer (2002). Observation of the Earth and its Environment: Survey of Missions and Sensors (4th Ed.).

References I

M. P. Bailey and J. Hallett. A Comprehensive Habit Diagram for Atmospheric Ice Crystals: Confirmation from the Laboratory, AIRS II, and Other Field Studies. *Journal of the Atmospheric Sciences*, 66(9):2888 – 2899, 2009. URL https://doi.org/10.1175/2009JAS2883.1.

O. Boucher. *Atmospheric Aerosols*. Springer Netherlands, 2015. URL https://doi.org/10.1007%2F978-94-017-9649-1.

B. J. Finlayson-Pitts and J. N. Pitts. *Chemistry of the Upper and Lower Atmosphere*. Academic Press, San Diego, 2000. ISBN 978-0-12-257060-5. URL https://doi.org/10.1016/B978-012257060-5/50003-4.

N. P. Gillett, M. Kirchmeier-Young, A. Ribes, H. Shiogama, G. C. Hegerl, R. Knutti, G. Gastineau, J. G. John, L. Li, L. Nazarenko, N. Rosenbloom, Ø. Seland, T. Wu, S. Yukimoto, and T. Ziehn. Constraining human contributions to observed warming since the pre-industrial period. *Nature Climate Change*, 11(3):207–212, jan 2021. URL https://doi.org/10.1038%2Fs41558-020-00965-9.

P. Kuma. Visualising Data from CloudSat and CALIPSO Satellites, 2010. URL https://doi.org/10.5281/zenodo.3764234.

P. Kuma, A. J. McDonald, O. Morgenstern, R. Querel, I. Silber, and C. J. Flynn. Ground-based lidar processing and simulator framework for comparing models and observations (ALCF 1.0). *Geoscientific Model Development*, 14(1):43–72, 2021. URL https://doi.org/10.5194/gmd-14-43-2021.

A. P. Lock, A. R. Brown, M. R. Bush, G. M. Martin, and R. N. B. Smith. A New Boundary Layer Mixing Scheme. Part I: Scheme Description and Single-Column Model Tests. *Monthly Weather Review*, 128(9):3187 – 3199, 2000. URL https://doi.org/10.1175/1520-0493(2000)128<3187:ANBLMS>2.0.CO;2.

G. G. Mace and A. Protat. Clouds over the Southern Ocean as Observed from the R/V Investigator during CAPRICORN. Part I: Cloud Occurrence and Phase Partitioning. *Journal of Applied Meteorology and Climatology*, 57(8):1783 – 1803, 2018. URL https://doi.org/10.1175/JAMC-D-17-0194.1.

V. Masson-Delmotte, P. Zhai, A. Pirani, S. Connors, C. Péan, S. Berger, N. Caud, Y. Chen, L. Goldfarb, M. Gomis, M. Huang, K. Leitzell, E. Lonnoy, J. Matthews, T. Maycock, T. Waterfield, O. Yelekçi, R. Yu, and B. Zhou, editors. *Climate Change 2021: The Physical Science Basis. Contribution of Working Group I to the Sixth Assessment Report of the Intergovernmental Panel on Climate Change*. Cambridge University Press, Cambridge, United Kingdom, 2021. In press.

A. V. Matus and T. S. L'Ecuyer. The role of cloud phase in Earth's radiation budget. *Journal of Geophysical Research: Atmospheres*, 122(5):2559–2578, 2017. URL https://doi.org/10.1002/2016JD025951.

References II

A. H. Omar, D. M. Winker, M. A. Vaughan, Y. Hu, C. R. Trepte, R. A. Ferrare, K.-P. Lee, C. A. Hostetler, C. Kittaka, R. R. Rogers, R. E. Kuehn, and Z. Liu. The CALIPSO Automated Aerosol Classification and Lidar Ratio Selection Algorithm. *Journal of Atmospheric and Oceanic Technology*, 26(10):1994 – 2014, 2009. URL https://doi.org/10.1175/2009JTECHA1231.1.

G. W. Petty. *A First Course in Atmospheric Radiation*. Sundog Publishing, 2 edition, 2006. ISBN 978-0972903318.

L. E. Revell, P. Kuma, E. C. L. Ru, W. R. C. Somerville, and S. Gaw. Direct radiative effects of airborne microplastics. *Nature*, 598(7881):462–467, oct 2021. URL https://doi.org/10.1038%2Fs41586-021-03864-x.

G. Shaddick, M. L. Thomas, P. Mudu, G. Ruggeri, and S. Gumy. Half the world's population are exposed to increasing air pollution. *npj Climate and Atmospheric Science*, 3(1), jun 2020. URL https://doi.org/10.1038%2Fs41612-020-0124-2.

S. C. Sherwood, M. J. Webb, J. D. Annan, K. C. Armour, P. M. Forster, J. C. Hargreaves, G. Hegerl, S. A. Klein, K. D. Marvel, E. J. Rohling, M. Watanabe, T. Andrews, P. Braconnot, C. S. Bretherton, G. L. Foster, Z. Hausfather, A. S. von der Heydt, R. Knutti, T. Mauritsen, J. R. Norris, C. Proistosescu, M. Rugenstein, G. A. Schmidt, K. B. Tokarska, and M. D. Zelinka. An Assessment of Earth's Climate Sensitivity Using Multiple Lines of Evidence. *Reviews of Geophysics*, 58(4): e2019RG000678, 2020. URL https://doi.org/10.1029/2019RG000678.

C. J. Smith, G. R. Harris, M. D. Palmer, N. Bellouin, W. Collins, G. Myhre, M. Schulz, J.-C. Golaz, M. Ringer, T. Storelvmo, and P. M. Forster. Energy Budget Constraints on the Time History of Aerosol Forcing and Climate Sensitivity. *Journal of Geophysical Research: Atmospheres*, 126(13):e2020JD033622, 2021. URL https://doi.org/10.1029/2020JD033622.

R. N. B. Smith. A scheme for predicting layer clouds and their water content in a general circulation model. *Quarterly Journal of the Royal Meteorological Society*, 116(492):435–460, 1990. URL https://doi.org/10.1002/qj.49711649210.

T. Stocker, D. Qin, G.-K. Plattner, M. Tignor, S. Allen, J. Boschung, A. Nauels, Y. Xia, V. Bex, and P. Midgley, editors. *Climate Change 2013: The Physical Science Basis. Contribution of Working Group I to the Fifth Assessment Report of the Intergovernmental Panel on Climate Change*. Cambridge University Press, Cambridge, United Kingdom and New York, NY, USA, 2013.

C. Wang, B. J. Soden, W. Yang, and G. A. Vecchi. Compensation Between Cloud Feedback and Aerosol-Cloud Interaction in CMIP6 Models. *Geophysical Research Letters*, 48(4):e2020GL091024, 2021. URL https://doi.org/10.1029/2020GL091024.

References III

D. Wang, I. S. Stachlewska, J. Delanoë, D. Ene, X. Song, and D. Schüttemeyer. Spatio-temporal discrimination of molecular, aerosol and cloud scattering and polarization using a combination of a Raman lidar, Doppler cloud radar and microwave radiometer. *Opt. Express*, 28(14):20117–20134, Jul 2020. URL `https://doi.org/10.1364/OE.393625`.

M. D. Zelinka, S. A. Klein, and D. L. Hartmann. Computing and Partitioning Cloud Feedbacks Using Cloud Property Histograms. Part I: Cloud Radiative Kernels. *Journal of Climate*, 25(11):3715 – 3735, 2012. URL `https://doi.org/10.1175/JCLI-D-11-00248.1`.